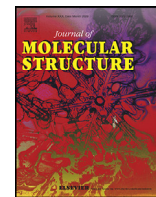




Contents lists available at ScienceDirect

Journal of Molecular Structure

journal homepage: www.elsevier.com/locate/molstr

Synthesis, X-ray characterization, Hirshfeld surface analysis and DFT calculations on tetrazolyl-phenol derivatives: H-bonds vs C-H...π/π...π interactions

Asma Bibi^a, Imtiaz Khan^{b,*}, Hina Andleeb^{a,c}, Jim Simpson^d, Muhammad Nawaz Tahir^e, Shahid Hameed^{a,*}, Antonio Frontera^{f,*}

^a Department of Chemistry, Quaid-i-Azam University, Islamabad-45320, Pakistan

^b Department of Chemistry and Manchester Institute of Biotechnology, The University of Manchester, 131 Princess Street, Manchester M1 7DN, United Kingdom

^c Sulaiman Bin Abdullah Aba Al-Khail – Centre for Interdisciplinary Research in Basic Science (SA-CIRBS), Faculty of Basic and Applied Sciences, International Islamic University, Islamabad, Pakistan

^d Department of Chemistry, University of Otago, P.O. Box 56, Dunedin, 9054, New Zealand

^e Department of Physics, University of Sargodha, Sargodha, Pakistan

^f Departament de Química, Universitat de les Illes Balears, Ctra de Valldemossa km 7.5, 07122 Palma de Mallorca (Baleares), Spain

ARTICLE INFO

Article history:

Received 24 August 2020

Revised 5 October 2020

Accepted 7 October 2020

Available online xxx

Keywords:

Non-covalent interactions

Hirshfeld surface analysis, Tetrazoles

DFT calculations

QTAIM

ABSTRACT

Tetrazoles are nitrogen rich heterocycles with a broad spectrum of medicinal properties and potential for use as drugs. A significant number of FDA approved drugs incorporate the tetrazole moiety indicating the versatile pharmaceutical potential associated with this heteroaromatic skeleton. Owing to the higher number of nitrogen atoms and σ-lone pairs, tetrazoles offer the opportunity to control structural topology through non-covalent interactions. In this perspective, the present research is focused on the investigation of various non-covalent interactions in a series of tetrazole derivatives (**5a–c**) incorporating a linear aliphatic chain (eight to fifteen carbon atoms) at N-2 and with a phenol moiety at the only carbon atom of the tetrazole ring. The detailed X-ray crystallographic investigations revealed the formation of various supramolecular architectures employing non-covalent interactions of a diverse nature. Further insights into these intermolecular interactions were obtained using Hirshfeld surface analysis and DFT calculations focusing on the H-bonds, C-H...π and π-π interactions in the structures. These contacts have been characterized by combining the quantum theory of “atoms-in-molecules” (QTAIM) with the non-covalent interaction index (NCIplot).

© 2020 Elsevier B.V. All rights reserved.

1. Introduction

Tetrazoles are doubly unsaturated five-membered aromatic heterocycles featuring one carbon and four nitrogen atoms and are ranked among the stable heterocycles with highest number of nitrogen atoms. However, pentazoles are highly explosive azaheterocycles [1]. Tetrazoles can accommodate a maximum of three pendant groups on the ring. Substituted tetrazoles with 6π electrons may exist in two tautomeric forms shown in I or II (Fig. 1) [2–4].

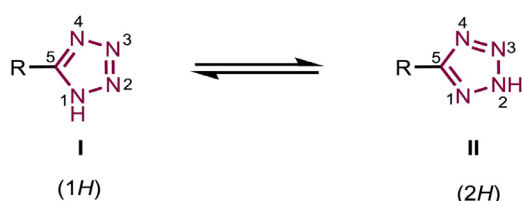
They show diverse properties such as bioisosterism [5] to carboxylic acid and amide functionalities alongside metabolic stability [6,7] and a good physicochemical character in the form of spatial

delocalization of the negative charge. They also exhibit good membrane penetration and enhanced lipophilicity [8,9], and take a central place in the medicinal chemistry and drug discovery arenas displaying a plethora of biological applications [10–27]. The pharmaceutical significance of these heterocycles is well reflected in the data obtained from Drug Bank [28] indicating 43 drugs with 1H- or 2H-tetrazole moieties, 23 of which are FDA approved [29]. Tetrazoles offer more opportunities to establish hydrogen bonds or π-stacking with the receptor recognition sites due to the higher number of nitrogen atoms and σ-lone pairs [30]. Moreover, tetrazoles can also be employed as ligands in coordination chemistry [31,32] and for the synthesis of liquid crystals [33]. Fig. 2 illustrates representative examples of drug molecules and liquid crystals highlighting the tetrazole functionality [29,33].

Non-covalent interactions, also known as “supramolecular interactions”, have gained eminence due to their conspicuous role in

* Corresponding authors.

E-mail addresses: imtiaz.khan@manchester.ac.uk (I. Khan), shameed@qau.edu.pk (S. Hameed), toni.frontera@uib.es (A. Frontera).

**Fig. 1.** Tautomerism of tetrazole derivatives.

several leading areas of modern research ranging from supramolecular chemistry to molecular biology [34–37], particularly in drug–receptor interactions, enzyme inhibition and protein folding [38]. Other applications include the management of the structures of biomolecules such as proteins and DNA, several host–guest systems, and enzyme–substrate binding [39,40]. Recognizing the importance of non-covalent interactions such as hydrogen bonding, halogen bonding, van der Waals forces, π – π stacking, cation– π , C–H... π , $\text{I}^{\text{p}}\text{–}\pi$, anion– π and metallophilic interactions [41–45] in small organic molecules and proteins, extensive investigations have been performed [46,47]. Despite their small magnitude such contacts exert a significant impact on structural topology thus affecting several physical and chemical characteristics of bio-systems [48–52]. Within the field of crystal engineering, an understanding of crystal packing is sought by a detailed knowledge of intermolecular interactions [47] leading to understanding and control of self-assembly and molecular recognition [53–55].

In view of the ubiquitous nature and unique role in diverse fields, the investigation and understanding of these weak non-covalent interactions have emerged as one of the major objectives of contemporary chemistry. Consequently, several researchers have documented and analyzed various non-covalent interactions using combined theoretical and experimental methods [56–62] rendering it an interesting topic of research. In a continuation of our previous

efforts [63–66], in the present study, we report three new tetrazole molecules bearing a phenol and an alkylated chain that have been investigated for the formation of supramolecular assemblies involving various non-covalent interactions. In particular, the abilities of the tetrazole and phenol moieties as H-bond donor/acceptor groups and promoting π -stacking are studied and analyzed using DFT calculations and a combination of QTAIM and NCIplot computational tools.

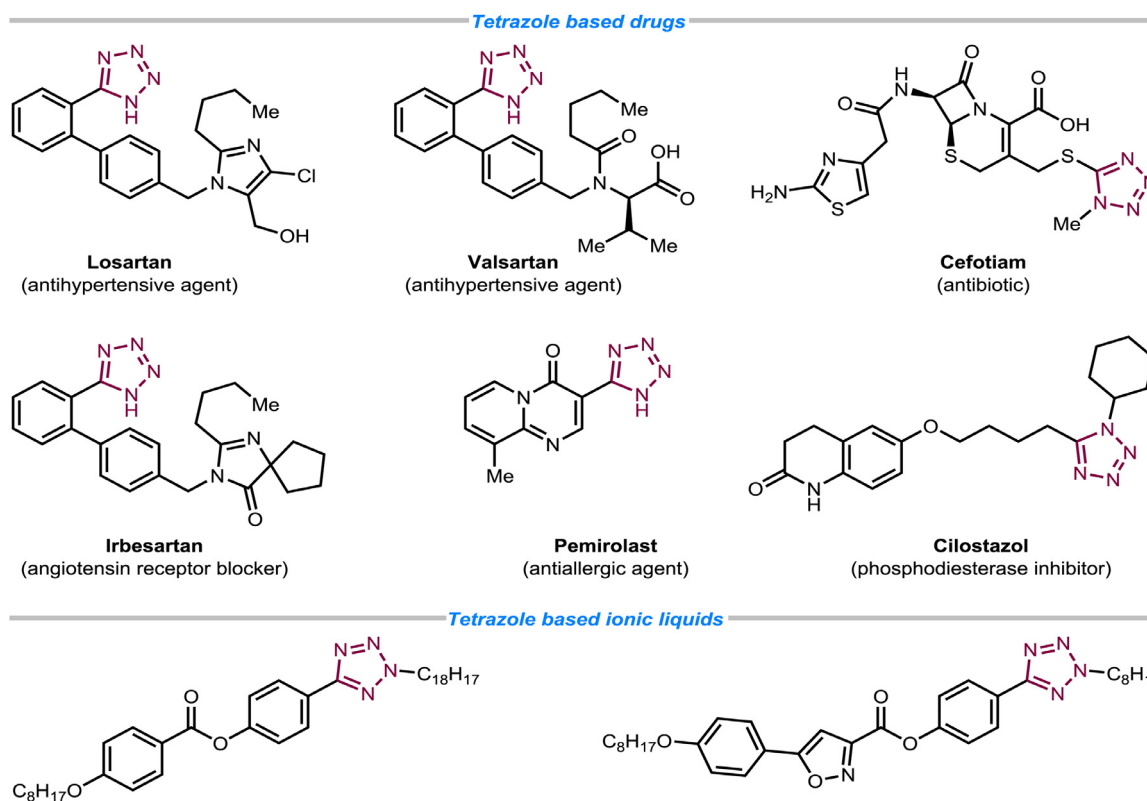
2. Experimental

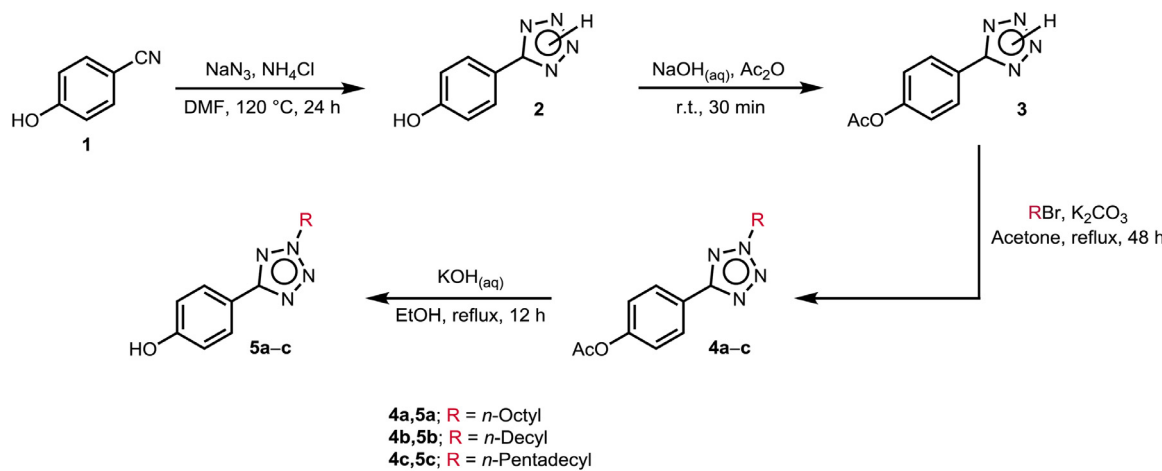
2.1. Instrumentation and techniques

The progress of all reactions was monitored by TLC using pre-coated silica gel-60 F₂₅₄ TLC plates purchased from Merck (Germany). Melting points of the synthesized compounds were determined in open capillaries using a Gallenkamp melting point (MPD) apparatus and are uncorrected. The FTIR spectra were performed on a Shimadzu Fourier Transform Infra-Red spectrophotometer model 270 using ATR (Attenuated total reflectance) facility. NMR spectra were recorded on a Bruker Avance 300 MHz spectrophotometer. ¹H and ¹³C NMR spectra were obtained using CDCl₃ as solvent with reference to TMS as internal standard.

2.2. Substrates and reagents

4-Cyanophenol, sodium azide, ammonium chloride, acetic anhydride, 1-bromoocetane, 1-bromodecane, 1-bromopentadecane and *N,N*-dimethylformamide (DMF) were purchased from Sigma-Aldrich (Germany). Tetrahydrofuran (THF) and methanol were supplied by Lab-Scan (Poland). Silica gel, dichloromethane (DCM), *n*-hexane and petroleum ether were purchased from Merck (Germany). Ethyl acetate was purchased from Ridel-de-Haën (USA). Anhydrous potassium carbonate (K₂CO₃) and magnesium sulfate

**Fig. 2.** Representative examples of biologically active drugs (top) and liquid crystals (bottom) highlighting tetrazole functionality.

**Scheme 1.** Synthetic route to 2,5-disubstituted tetrazoles (5a-c).

(MgSO₄) were obtained from WINLAB (USA). Ethanol and acetone were obtained from commercial sources. The reagents used were of analytical grade and the commercial solvents were distilled before use.

2.3. Synthetic chemistry

The numbering of the various starting materials used in these syntheses is shown in Scheme 1.

2.3.1. Preparation of 4-(2H-tetrazol-5-yl)phenol (2)

To a stirred solution of 4-cyanophenol **1** (10.0 g, 0.084 mol) in N,N-dimethylformamide (50 mL) was added sodium azide (22.0 g, 0.340 mol) followed by ammonium chloride (18.0 g, 0.340 mol). The mixture was heated to 120 °C for 24 h. The reaction mixture was cooled to room temperature, poured onto ice cold water (50 mL) and acidified with aqueous HCl to pH 2. The precipitated solid was filtered and crystallized (ethanol) to afford 4-(2H-tetrazol-5-yl)phenol **2** in 78% yield [67]. m.p.: 238.0–238.8 °C; R_f = 0.23 (40% EtOAc in *n*-hexane); FTIR (neat, ν_{max}, cm⁻¹): 3445, 3254, 3030, 1608; ¹H NMR (300 MHz, CDCl₃): δ (ppm) 8.1 (2H, d, J = 6.6 Hz), 7.3 (2H, d, J = 6.6 Hz); ¹³C NMR (75 MHz, CDCl₃): δ (ppm) 169.4, 152.2, 127.3, 125.5, 122.6.

2.3.2. Preparation of 4-(2H-tetrazol-5-yl)phenyl acetate (3)

To an ice-cold solution of sodium hydroxide (3 M, 27.6 mL) was added 4-(2H-tetrazol-5-yl)phenol **2** (5.4 g, 0.033 mol) followed by acetic anhydride (7.9 mL, 0.083 mol). The reaction mixture was vigorously stirred for 30 min and the precipitated solid was filtered, washed with cold water and crystallized from a mixture of water-methanol to afford 4-(2H-tetrazol-5-yl)phenyl acetate **3** as a white solid in 75% yield [67]. m.p.: 186.3–187.4 °C; R_f = 0.33 (40% EtOAc in *n*-hexane); FTIR (neat, ν_{max}, cm⁻¹): 3254, 3075, 2938, 2844, 1758, 1613, 1504, 1207; ¹H NMR (300 MHz, CDCl₃): δ (ppm) 8.1 (2H, d, J = 6.6 Hz), 7.4 (2H, d, J = 6.6 Hz), 2.3 (3H, s); ¹³C NMR (75 MHz, CDCl₃): δ (ppm) 169.0, 158.0, 153.0, 128.0, 125.2, 122.4, 22.9.

2.3.3. General procedure for the preparation of

4-[2-(alkyl)-2H-tetrazol-5-yl]phenyl acetate (4a-c)

To a stirred mixture of 4-(2H-tetrazol-5-yl)phenyl acetate **3** (5.0 g, 24 mmol) and anhydrous K₂CO₃ (3.30 g, 24 mmol) in acetone (40 mL) was added appropriate alkyl halide (24 mmol) and the mixture was heated to reflux for 48 h. The reaction mixture was cooled to room temperature and filtered to remove excess K₂CO₃. The solvent was removed in vacuo and the product was crystallized from ethanol [67].

2.3.3.1. 4-[(2-Octyl)-2H-tetrazol-5-yl]phenyl acetate (4a). White solid (yield: 51%); R_f = 0.76 (30% EtOAc in *n*-hexane); FTIR (neat, ν_{max}, cm⁻¹): 2942, 2851, 1758, 1613, 1207, 1171, 918; ¹H NMR (300 MHz, CDCl₃): δ (ppm) 8.2 (2H, d, J = 8.8 Hz), 7.2 (2H, d, J = 8.8 Hz), 4.6 (2H, t, J = 7.2 Hz), 2.3 (3H, s), 2.1 (2H, quint, J = 7.2 Hz), 1.8–1.3 (10H, m), 0.9 (3H, t, J = 6.9 Hz); ¹³C NMR (CDCl₃): δ (ppm) 169.4, 164.5, 152.3, 128.2, 125.4, 122.3, 53.4, 31.8, 29.5, 29.2, 29.0, 26.5, 22.8, 21.4, 14.2.

2.3.3.2. 4-[(2-Decyl)-2H-tetrazol-5-yl]phenyl acetate (4b). White solid (yield: 50%); R_f = 0.78 (30% EtOAc in *n*-hexane); FTIR (neat, ν_{max}, cm⁻¹): 2951, 2851, 1750, 1614, 1222, 1177, 918; ¹H NMR (300 MHz, CDCl₃): δ (ppm) 8.2 (2H, d, J = 8.7 Hz), 7.3 (2H, d, J = 8.7 Hz), 4.6 (2H, t, J = 7.2 Hz), 2.3 (3H, s), 2.1 (2H, quint, J = 7.2 Hz), 1.5–1.2 (14H, m), 0.9 (3H, t, J = 7.0 Hz); ¹³C NMR (CDCl₃): δ (ppm) 169.2, 164.3, 152.1, 128.5, 125.2, 122.1, 53.3, 31.8, 29.6, 29.4, 29.3, 29.2, 28.8, 26.3, 22.6, 21.2, 14.2.

2.3.3.3. 4-[(2-Pentadecyl)-2H-tetrazol-5-yl]phenyl acetate (4c). White solid (yield: 56%); R_f = 0.83 (30% EtOAc in *n*-hexane); FTIR (neat, ν_{max}, cm⁻¹): 2926, 2857, 1753, 1615, 1230, 1169, 914; ¹H NMR (300 MHz, CDCl₃): δ (ppm) 8.2 (2H, d, J = 8.7 Hz), 7.3 (2H, d, J = 8.7 Hz), 4.6 (2H, t, J = 7.2 Hz), 2.3 (3H, s), 2.1 (2H, quint, J = 7.2 Hz), 1.5–1.2 (24H, m), 0.9 (3H, t, J = 7.0 Hz); ¹³C NMR (CDCl₃): δ (ppm) 169.1, 164.2, 152.0, 128.5, 125.2, 122.1, 53.3, 31.8, 29.6, 29.4, 29.3, 29.1, 29.0, 28.9, 28.8, 26.5, 26.3, 22.7, 21.2, 19.1, 14.1, 13.7.

2.3.4. General method for the deprotection reaction

To a stirred solution of 4-[2-(alkyl)-2H-tetrazol-5-yl]phenyl acetate **4a-c** (6.2 mmol) in methanol (20 mL) was added KOH (0.346 g, 6.2 mmol) in water (10 mL) and the resulting mixture was heated to reflux for 12 h. After completion of the reaction, the mixture was cooled to room temperature, filtered and volatiles were removed under reduced pressure. The residue was poured onto ice (100 g) and acidified with aqueous HCl to pH 2. The precipitated solid was filtered and recrystallized from ethanol to afford compounds **5a-c** [67].

2.3.4.1. 4-[(2-Octyl)-2H-tetrazol-5-yl]phenol (5a). White crystalline solid (yield: 59%); m.p.: 65.5–66 °C; R_f = 0.85 (30% EtOAc in *n*-hexane); FTIR (neat, ν_{max}, cm⁻¹): 3363, 2933, 2849, 1615, 1171, 853; ¹H NMR (300 MHz, CDCl₃): δ (ppm) 7.9 (2H, d, J = 8.7 Hz), 6.9 (2H, d, J = 8.7 Hz), 6.7 (1H, s), 4.2 (2H, t, J = 7.2 Hz), 1.8 (2H, quint, J = 7.2 Hz), 1.4–1.2 (10H, m), 0.9 (3H, t, J = 5.8 Hz); ¹³C NMR (CDCl₃): δ (ppm) 165.2, 158.0, 128.8, 120.0, 116.1, 53.4, 31.9, 29.6, 29.3, 28.9, 26.6, 22.8, 14.3.

2.3.4.2. 4-[(2-Decyl)-2H-tetrazol-5-yl]phenol (5b). White crystalline solid (yield: 75%); m.p.: 73.4–76.3 °C; R_f = 0.86 (30% EtOAc in *n*-hexane); FTIR (neat, ν_{max} , cm⁻¹): 3409, 2941, 2854, 1620, 1169, 845; ¹H NMR (300 MHz, CDCl₃): δ (ppm) 7.9 (2H, d, *J* = 8.8 Hz), 7.0 (2H, d, *J* = 8.7 Hz), 6.7 (1H, s), 4.6 (2H, t, *J* = 7.2 Hz), 1.8 (2H, quint, *J* = 7.2 Hz), 1.4–1.2 (14H, m), 0.9 (3H, t, *J* = 5.9 Hz); ¹³C NMR (75 MHz, CDCl₃): δ (ppm) 164.9, 160.8, 128.3, 119.9, 114.8, 53.1, 31.8, 29.6, 29.3, 28.9, 26.4, 22.7, 19.1, 18.7, 14.2.

2.3.4.3. 4-[(2-Pentadecyl)-2H-tetrazol-5-yl]phenol (5c). White crystalline solid (yield: 64%); m.p.: 74–76 °C; R_f = 0.87 (30% EtOAc in *n*-hexane); FTIR (neat, ν_{max} , cm⁻¹): 3338, 2930, 2850, 1610, 1174, 855; ¹H NMR (300 MHz, CDCl₃): δ (ppm) 8.0 (2H, d, *J* = 9.0 Hz), 6.9 (2H, d, *J* = 8.7 Hz), 6.7 (1H, s), 4.6 (2H, t, *J* = 7.2 Hz), 2.0 (2H, quint, *J* = 7.2 Hz), 1.3–1.2 (24H, m), 0.9 (3H, t, *J* = 6.7 Hz); ¹³C NMR (75 MHz, CDCl₃): δ (ppm) 164.8, 157.9, 128.5, 119.6, 115.9, 53.2, 31.9, 29.6, 29.4, 29.3, 29.1, 29.0, 28.9, 28.8, 26.5, 26.3, 22.7, 19.1, 19.0, 14.1.

2.4. Crystal growth development

Single crystals of compounds **5a–c** suitable for X-ray diffraction analysis were grown at room temperature from ethanol as the solvent.

2.5. X-ray structure determination

Crystallographic data for compounds **5a–c** are listed in Table 1. Diffraction data were collected on a Bruker APEXII CCD diffractometer using graphite-monochromated Mo-K α radiation

(λ = 0.71073 Å). Data collections were controlled by APEX2 software [68] with cell refinement and data reduction performed using SAINT [68]. Multi-scan absorption corrections were applied using SADABS [69]. The structures were solved with SHELXS-97 [70] and refined by full-matrix least-squares on F² using SHELXL-2018/1 [71] and TITAN2000 [72]. All non-hydrogen atoms were assigned anisotropic displacement parameters. All H-atoms were positioned geometrically and refined using a riding model with d(O-H) = 0.84 Å and U_{iso} = 1.5U_{eq}(O), d(C-H) = 0.93 for aromatic and 0.97 Å for CH₂ with U_{iso} = 1.2U_{eq}(C) and 0.96 Å, U_{iso} = 1.5U_{eq}(C) for CH₃ atoms. **5b** crystallizes in a non-centric space group, P2₁2₁2₁, but the absolute structure cannot be determined reliably, and the Flack parameter is not reported. All molecular plots and packing diagrams were drawn using Mercury [73]. Other calculations were performed using PLATON [74] and the tabular material was produced using WINGX [75].

2.6. Theoretical methods

The energies of the complexes included in this study were computed at the PBE1PBE-D3/def2-TZVP level of theory by using the program Gaussian-16 [76]. The interaction energy (or binding energy in this work) ΔE , is defined as the energy difference between the multicomponent assembly and the sum of the energies of the monomers, unless otherwise noted. The basis set superposition error has been corrected using the counterpoise method [77]. For the calculations we have used the Weigend def2-TZVP [78,79] basis set and the PBE1PBE DFT functional [80,81]. Grimme's D3 dispersion correction has been used [82,83] to better estimate the π - π interactions. The MEP (Molecular Electrostatic Potential) surfaces calculations have been computed using Gaussian-16 software at the PBE1PBE-D3/def2-TZVP level of theory and using the 0.001 a.u.

Table 1

Crystal data and structure refinement for **5a–c**.

Compound	5a	5b	5c
Empirical formula	C ₁₅ H ₂₂ N ₄ O	C ₁₇ H ₂₆ N ₄ O	C ₂₂ H ₃₆ N ₄ O
Formula weight	274.36	302.42	372.55
Temperature (K)	296(2)	296(2)	296(2)
Wavelength (Å)	0.71073	0.71073	0.71073
Crystal system	Monoclinic	Orthorhombic	Monoclinic
Space group	P2 ₁ /n	P2 ₁ 2 ₁ 2 ₁	P2 ₁ /n
<i>a</i> (Å)	9.7352(5)	13.4508(8)	6.0774(4)
<i>b</i> (Å)	13.1170(7)	18.6627(14)	9.6725(7)
<i>c</i> (Å)	12.4010(7)	21.5332(17)	37.496(3)
α (°)	90	90	90
β (°)	98.237(2)	90	91.924(3)
γ (°)	90	90	90
Volume (Å ³)	1567.23(15)	5405.4(7)	2202.9(3)
Z	4	12	4
D _{calcd} (g cm ⁻³)	1.163	1.115	1.123
μ (mm ⁻¹)	0.076	0.072	0.070
Crystal size(mm)	0.42 × 0.34 × 0.30	0.43 × 0.24 × 0.20	0.36 × 0.32 × 0.26
Theta range for data collection (°)	2.273 to 27.523	1.444 to 25.497	2.174 to 26.870
Index ranges	-12 <= <i>h</i> <= 12, -17 <= <i>k</i> <= 16, -16 <= <i>l</i> <= 15	-16 <= <i>h</i> <= 14, -22 <= <i>k</i> <= 22, -26 <= <i>l</i> <= 26	-7 <= <i>h</i> <= 7, -12 <= <i>k</i> <= 12, -47 <= <i>l</i> <= 47
Reflections collected	13,383	41,463	18,279
Independent reflections	3569 [R(int) = 0.0221]	10,075 [R(int) = 0.0723]	4748 [R(int) = 0.0373]
Completeness to theta = 25.242°	100.0%	100.0%	100.0%
Refinement method	Full-matrix least-squares on F ²		
Min. and max. transmission	0.670 and 0.746	0.945 and 0.978	0.975 and 0.982
Data/restraints/parameters	3569 / 0 / 183	10,075 / 0 / 601	4748 / 0 / 249
Goodness-of-fit on F ²	1.031	0.962	1.026
Final R indices [<i>I</i> > 2σ(<i>I</i>)]	R1 = 0.0418, wR2 = 0.1094	R1 = 0.0526, wR2 = 0.1009	R1 = 0.0491, wR2 = 0.1189
R indices (all data)	R1 = 0.0623, wR2 = 0.1232	R1 = 0.1445, wR2 = 0.1320	R1 = 0.0755, wR2 = 0.1313
Absolute structure parameter	-	-0.3(10)	-
Extinction coefficient	-	-	0.0213(14)
Largest difference peak and hole (e Å ⁻³)	0.162 and -0.187	0.137 and -0.200	0.186 and -0.148
CCDC reference number	988,868	999,009	999,010

envelope to generate the surface. The NCIPlot [84,85] index and QTAIM analyses have been performed using the PBE1PBE-D3/def2-TZVP wave function and the AIMALL program [86].

3. Results and discussion

3.1. Synthetic chemistry

The substituted tetrazoles **5a–c** were prepared using a four-step synthetic approach as outlined in [Scheme 1](#). In the first step, 1,3-dipolar cycloaddition of the azide anion with 4-cyanophenol **1** afforded tetrazole **2** in 78% yield which was acetylated using acetic anhydride to deliver compound **3** in 75% yield. Subsequently, the alkylation reaction of **3** with different alkyl bromides provided the corresponding *N*-2 alkylated tetrazoles **4a–c** which on basic hydrolysis afforded the target products **5a–c** in 59–75% isolated yields [67].

3.2. X-ray crystallography

As background to the structural investigation, a search of the Cambridge structural database [87] was conducted for the 5-phenyl-2-propyl-2*H*-tetrazole, C₆-CN₄CH₂CH₂ fragment in organic compounds. This resulted in 12 hits, none of which had an OH substituent at any position on the benzene ring. Two of the hits USE-BUR, (4-(2-ethyl-2*H*-tetrazol-5-yl)benzyl)phosphonic acid monohydrate [88] and KUVKOC, 1-(((cyclohexyloxy)carbonyl)oxy)ethyl 3-((2'-(2-ethyl-2*H*-tetrazol-5-yl)biphenyl-4-yl)methyl)-2-oxo-2,3-dihydro-1*H*-benzimidazole-4-carboxylate [89] have simple ethyl substituents on the 2-positions of the tetrazole rings. However extended alkyl chain substituents are found in MAZHED, 4-[4-(2-decyl-2*H*-tetrazol-5-yl)phenyl]-2,6-bis(1,3-thiazol-2-yl)pyridine [90] and two closely related compounds with hexyl and nonyl substituents on the tetrazole rings, UFITIO, 4-(2-hexyl-2*H*-tetrazol-5-yl)phenyl 4-(hexyloxy)benzoate and UFITEK 4-(2-nonyl-2*H*-tetrazol-5-yl)phenyl 4-(nonyloxy)benzoate [67]. The only other hit with a single tetrazole ring in the molecule was QIBLOF, butyl 4-(5-phenyl-2*H*-tetrazol-2-yl)butanoate [91]. The remaining hits have two tetrazole units in each molecule, link directly to a central benzene ring with bromoalkane chain of various lengths substituents on each of the tetrazole rings. Thus SARCAQ [92], has two bromo-ethyl chains, NUGBEX [93], bromo-propyl, while the isomeric NEMNAV, and NEMNEZ [94] have bromo-butyl chains. In the same paper NENNID is reported, with longer bromo-octyl substituents in each tetrazole ring [94].

The three compounds reported here, 4-(2-octyl-2*H*-tetrazol-5-yl)phenol, **5a**, 4-(2-decyl-2*H*-tetrazol-5-yl)phenol, **5b**, which crystallizes with 3 unique molecules (M1, M2 and M3) in the asymmetric unit, and 4-(2-pentadecyl-2*H*-tetrazol-5-yl)phenol, **5c** are closely similar, [Scheme 1](#), and their molecular structures can reasonably be discussed together. Each molecule features a tetrazole ring substituted on the N atom in the 2-position by beautifully ordered octyl, **5a**, decyl, **5b**, and pentadecyl, **5c**, alkane chains. In each case a phenol ring system is bound to the C atom at the 5-position of the tetrazole ring, [Fig. 3\(a–c\)](#).

The tetrazole and phenyl rings in **5a** are almost coplanar with a dihedral angle of 8.01(7)° between them with the O substituent of the phenol ring positioned 0.033(2) Å from the benzene ring plane ([Table 2](#)). The best fit mean plane through the 8 carbon atoms of the octyl substituent has a deviation of only 0.0642 Å and is inclined to the tetrazole ring plane by 15.7(1)°. The corresponding values for the three unique molecules of **5b** and those for **5c** also appear along [Table 2](#). While most of the angles and deviations are reasonably similar for all three molecules, the longer alkane is almost orthogonal to the plane of the tetrazole ring, unlike values of less than 16° for the other four molecules.

3.3. Crystal packing

In the crystals, packing is stabilized by a variety of hydrogen bonds, C–H...π contacts and a π...π stacking interactions.

3.3.1. Crystal packing of **5a**

In the crystal of **5a**, classical O1–H1...N4 hydrogen bonds supported by weaker C2–H2...O1 and C3–H3...N3 hydrogen bonds form zig-zag chains of molecules along *b*, [Fig. 4](#). C8–H8A...Cg2 hydrogen bonds form inversion related dimers that are linked by the O–H...C–H...O and C–H...N contacts mentioned previously into chains along *c*, [Fig. 5](#). Overall, these contacts stack molecules of **5a** along the *b* axis direction, [Fig. S1](#) in the supplementary material.

3.3.2. Crystal packing of **5b**

In the crystal of **5b**, O–H...N, C–H...O and C–H...N hydrogen bonds from both M1 and M2 molecules of **5b** form zig-zag chains along the *a* axis direction, [Fig. 6](#), in a fashion reminiscent of the packing found for **5a**, ([Fig. 4](#)). In contrast, M3 molecules link to one another, albeit in a very similar fashion with a similar set of hydrogen bonds, also forming zig-zag chains along *a*, [Fig. 7](#). M1, M2 and M3 molecules are linked along *c* by a variety of C–H...π contacts reinforced in one instance by a π...π interaction between the M1 and M3 tetrazole rings with centroid to centroid distances Cg1...Cg5 3.508(3) Å (symmetry operation 1–X, -1/2 + Y, 1/2–Z), [Fig. 8](#). The C–H...π contacts comprise C9–H9A...Cg6, H...C = 2.95 Å, (symmetry operation, 1–X, -1/2 + Y, 1/2–Z), C27–H27A...Cg2, H...C = 2.85 Å, (symmetry operation, -1 + X, Y, Z), C43–H43B...Cg2, H...C = 2.91 Å, (symmetry operation, 1–X, 1/2 + Y, 1/2–Z), C46–H46A...Cg3, H...C = 2.92 Å, (symmetry operation, X, Y, Z), [Fig. 8](#). Cg1, Cg2, Cg3, Cg5 and Cg6 are the centroids of the (N1, N2, N3, N4, C7); (C1–C6); (N5, N6, N7, N8, C24); (N9, N10, N11, N12, C41) and (C35–C40) rings respectively. These contacts combine to form approximately parallel sheets of M1, M2 and M3 molecules when viewed along the *a* axis direction, [Fig. S2](#) in the supplementary material.

3.3.3. Crystal packing of **5c**

In the crystal of **5c**, packing is stabilized by a variety of hydrogen bonds and a π...π stacking interaction. Strong classical O1–H1A...N3 form chains of molecules along *b*. Atom C8 adjacent to the tetrazole ring acts as a bifurcated donor with chains of molecules forming along the *a* axis direction as a result of both C8–H8A...N4 and C8–H8B...O1 contacts. Finally, weaker C5–H5...O1 hydrogen bonds firm dimers in the *ab* plane, with the C5–H5...O1 angle of approximately 137.6°. Each of these contacts are shown in [Fig. 9](#). π...π stacking interactions between the benzene and tetrazole rings are supported by the O1–H1A...N3 hydrogen bond forming a molecular trimer ([Fig. 10](#)) with Cg1...Cg2 centroid to centroid distances of 3.6719(9) Å. These contacts combine to form well separated stacks of molecules along the *b* axis direction ([Fig. S3](#)).

3.4. Hirshfeld analysis

Further details of the intermolecular interactions in the three molecules were obtained using Hirshfeld surface analysis [95] with surfaces and two-dimensional fingerprint plots generated by *CrystalExplorer* [96].

3.4.1. Hirshfeld analysis of **5a**

[Fig. 11](#) shows the Hirshfeld surface of the asymmetric unit of **5a**. The bold red circles in correspond to classical O–H...N hydrogen bonds with the weaker C–H...O contact appears as a faint red circle.

Fingerprint plots, [Fig. 12](#), show that H...H contacts are by far the most prolific with significant contributions also coming from

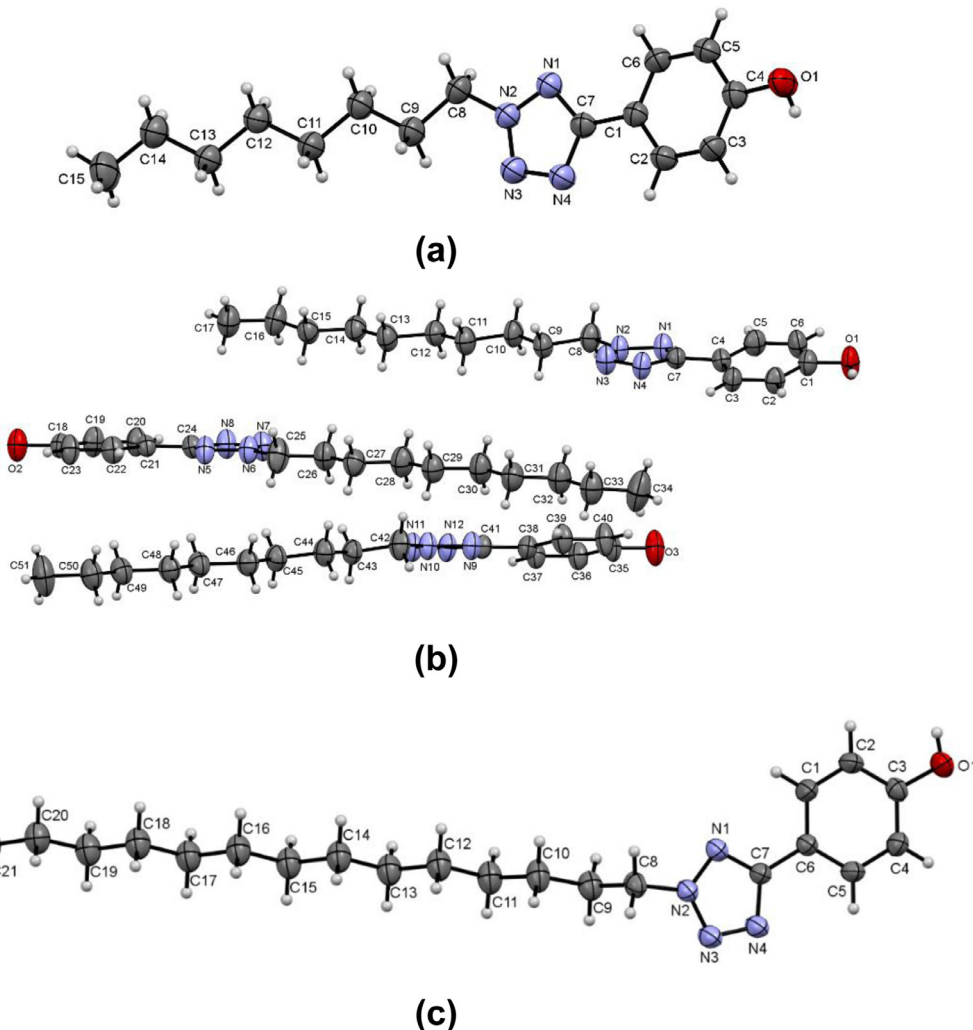


Fig. 3. (a) The molecular structure of **5a**, (b) the three molecules, M1, M2 and M3 that make up the asymmetric unit of **5b** and (c) the molecular structure of **5c** each showing the atom numbering schemes and with ellipsoids drawn at the 50% probability level.

Table 2

Metrical data for **5a**, **5b** and **5c**.

Molecule	Tetrazole/benzene angle (°)	O-H oxygen deviation (Å)	C _n chain rms deviation (Å)	C _n chain/tetrazole ring angle (°)
5a	8.01(7)	0.033(2)	0.0642	15.7(1)
5b, M1	13.24(13)	0.011(7)	0.0870	1.85(13)
5b, M2	1.708 (15)	0.011(8)	0.0681	4.31(2)
5c, M3	11.06(12)	-0.007 (7)	0.0439	5.34(10)
5c	5.27(6)	0.033(2)	0.0658	79.75(6)

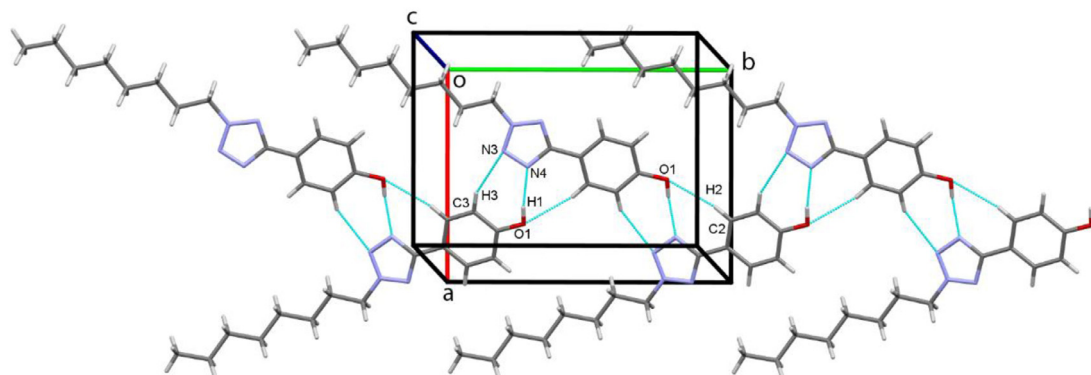


Fig. 4. Chains of molecules of **5a** along *b* with hydrogen bonds drawn as cyan dashed lines.

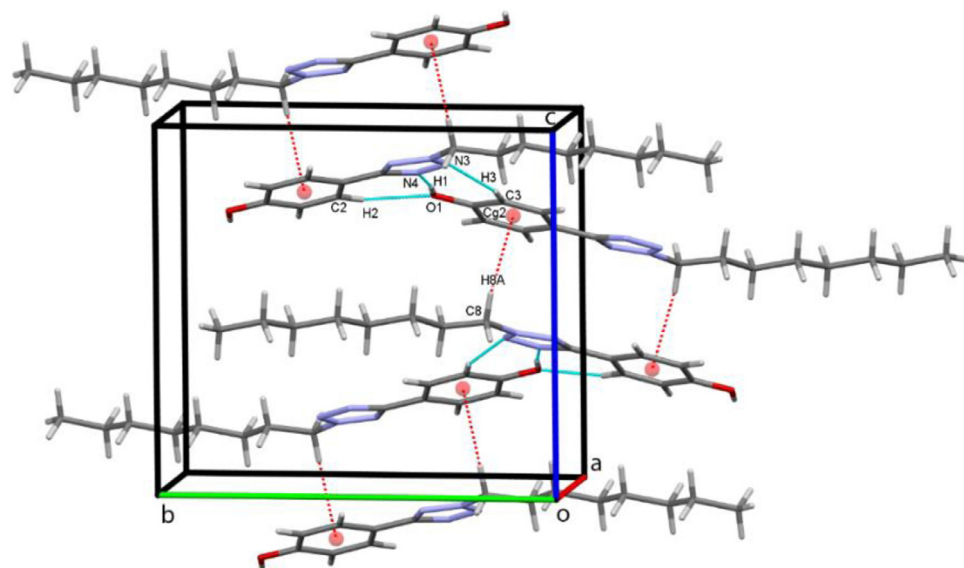


Fig. 5. Chains of C-H... π dimers along c . $Cg2$ is the centroid of the C1-C6 benzene ring and these are shown as red spheres, with C-H... π hydrogen bonds drawn as red dashed lines.

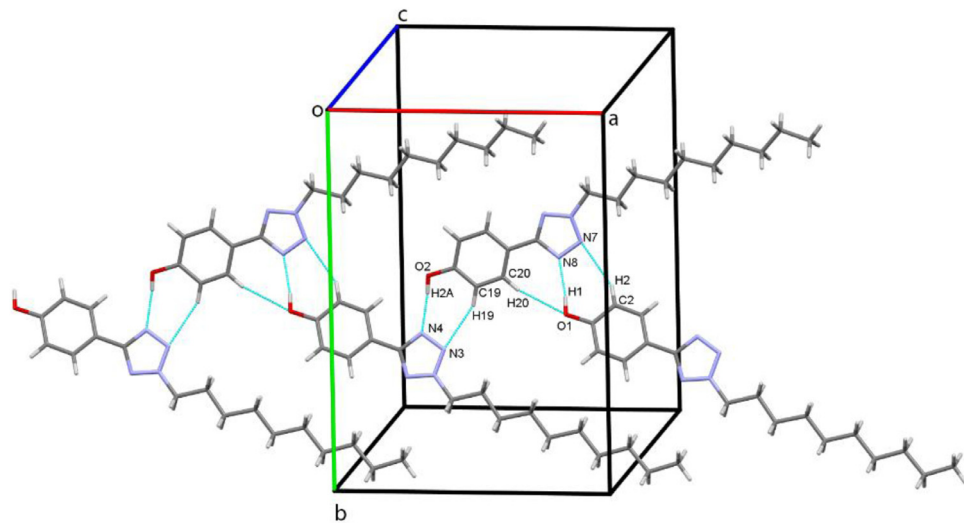


Fig. 6. Chains of molecules of **5b** along a involving both M1 and M2 molecules of **5b**.

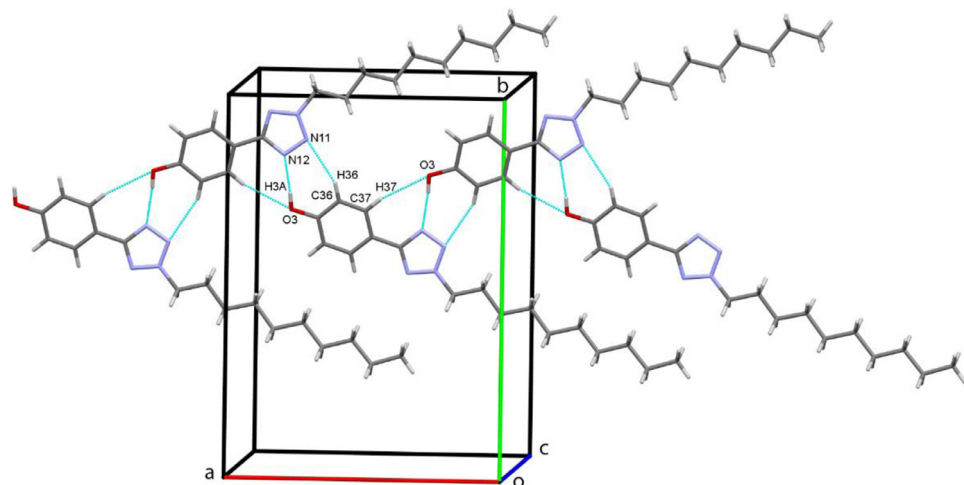


Fig. 7. A second set of chains of molecules of **5b** along a but in this instance only involving only M3 molecules.

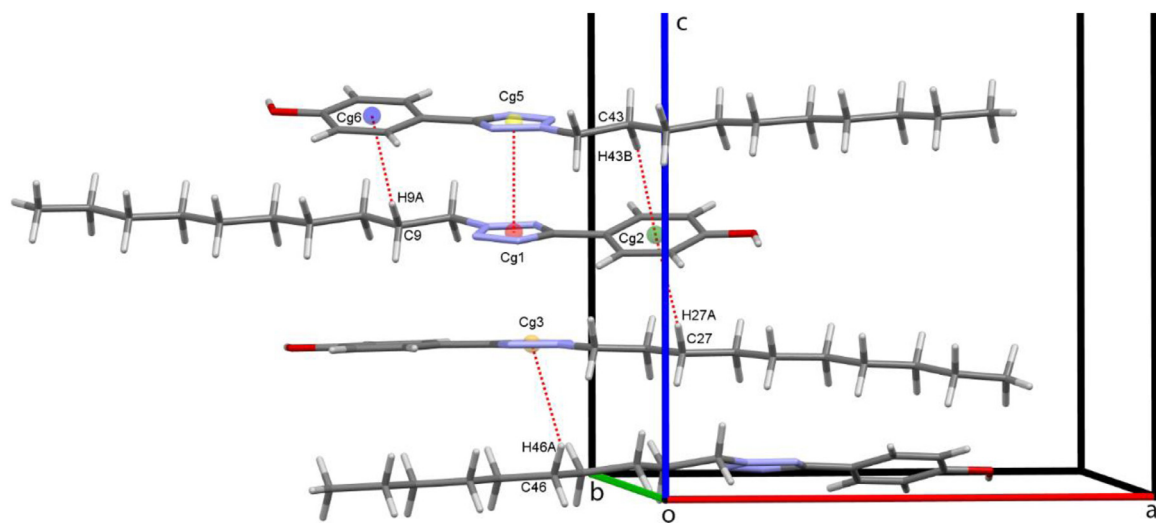


Fig. 8. $\pi \dots \pi$ and C–H... π contacts linking M1, M2 and M3 molecules of **5b** along *c*.

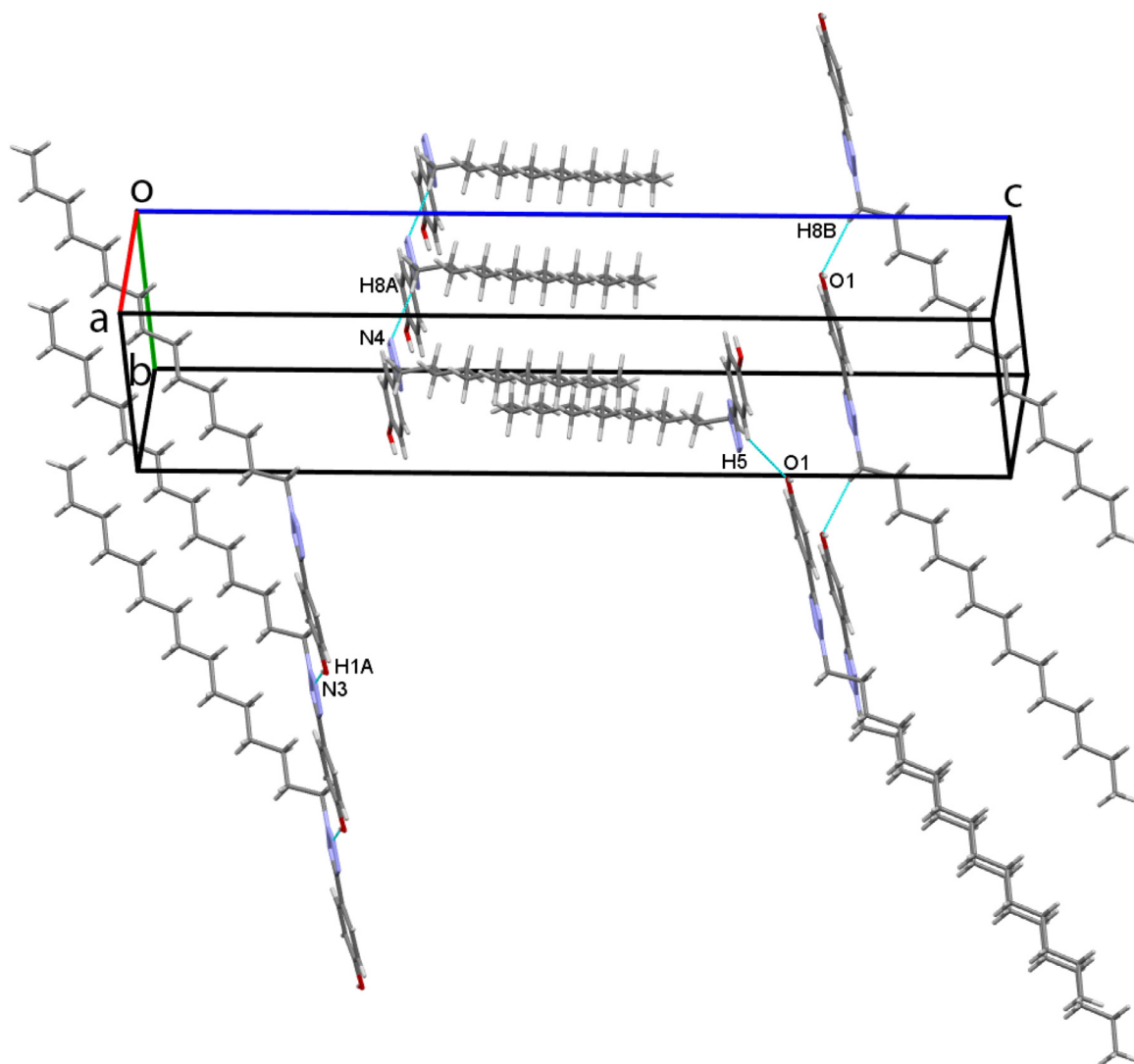


Fig. 9. The numerous hydrogen bonds formed by molecules of **5c**. O1-H1A...N3, far left, C8-H8A...N4, center top, C5-H5...O1 dimers, bottom center and C8-H8B...O1 hydrogen bonds, far right. For clarity, only the H donor and various acceptor atoms are labelled in this figure.

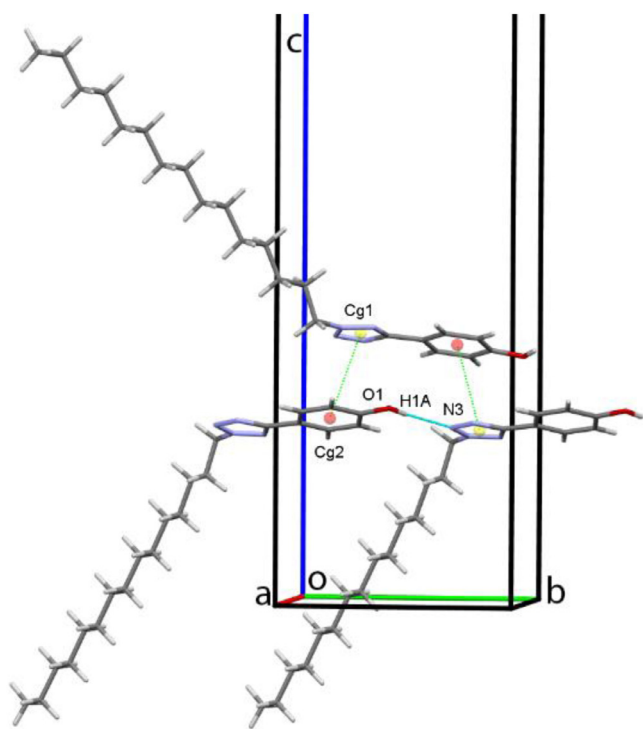


Fig. 10. Molecular trimers of **5c** formed by $\pi\ldots\pi$ stacking interactions between the benzene and tetrazole rings and supported by an O-H...N hydrogen bond.

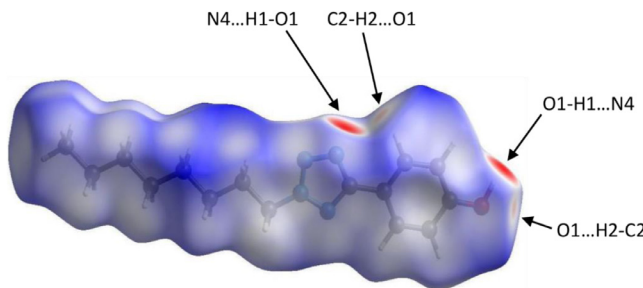


Fig. 11. Hirshfeld surfaces of the asymmetric unit of **5a**, mapped over d_{norm} in the range -0.5990 to 1.5925 a.u.

Table 3
Percentage contributions of interatomic contacts to the Hirshfeld surface for **5a-c**.

Contact	Included surface area (%)	5a	5b	5c
H...H	59.6	65.5	74.1	
H...C/C...H	14.3	13.2	8.1	
H...N/N...H	17.1	11.6	10.5	
H...O/O...H	7.1	7.2	3.8	
C...N	1.9	1.2	2.4	
N...N	-	1.2	-	
N...O	-	0.1	0.5	
C...O	-	-	0.3	
C...C	-	-	0.3	

H...N/N...H and H...C/C...H contacts. Weaker H...O/O...H and C...N interactions are also found, **Table 3**.

3.4.2. Hirshfeld analysis of **5b**

With three unique molecules in the asymmetric unit of **5b** the Hirshfeld analysis of this structure is more complex. We have therefore divided the analysis into four sections, examining first the complete asymmetric unit, followed by each of the unique

molecules 1, 2 and 3, M1, M2 and M3 individually. Results of this latter investigation are shown in the supplementary material (Figs. S4-S6).

3.4.2.1. Hirshfeld analysis of the asymmetric unit of **5b.** **Fig. 13** shows the Hirshfeld surfaces for the three molecules that form the asymmetric unit of **5b**. Strong O-H...N hydrogen bonds (bold red circles) dominate the surface contacts and are supported by weaker C-H...N hydrogen bonds, shown as smaller pale red circles.

Fingerprint plots, **Fig. 14**, show an even greater dominance of H...H contacts compared to that of **5a** no doubt reflecting the increased length of the alkyl chains in these molecules. The H...N/N...H contacts are considerably reduced compared to those in **5a** suggesting a degree of shielding of the tetrazole rings by the aggregation of the three unique molecules.

Hirshfeld analysis of the individual components of the asymmetric unit of **5b**, molecules M1, M2 and M3, is shown in the supplementary data. Again O-H...N and weaker C-H...N hydrogen bonds are found on the surfaces of each of the three molecules (Figs. S4-S6 and the corresponding fingerprint plots in Fig S7-S9). The three plots of the surfaces of the three unique molecules, perhaps unsurprisingly, look remarkably similar. Percentage contributions of interatomic contacts to the Hirshfeld surface for the three individual molecules of **5b** are detailed in Table S1.

3.4.3. Hirshfeld analysis of **5c**

Predictably O-H...N and weaker C-H...N hydrogen bonds are also found on the surface of this molecule further reflecting the close similarity of the three structures (**Fig. 15**).

A striking feature of the fingerprint plots for this molecule is the spectacular increase in the contribution of the H...H contacts to the included surface area at the expense of the other contacts. This undoubtedly reflects the significant extension of the alkyl chain to pentadecyl, providing the opportunity for additional H...H contacts (**Fig. 16**).

3.5. Theoretical (DFT) study

The study is focused to the analysis of the H-bonding and π -stacking interactions observed in the solid state of compounds **5a-c** that have been highlighted above in **Figs. 4-10**. First of all, we have computed the MEP surface of compound **5a** (**Fig. 17**), which also serves as a model of **5b,c**, to investigate the most electrophilic and nucleophilic parts of the molecule. It can be observed that the most positive MEP value is located at the phenolic H-atom (+52 kcal/mol) and, remarkably, the positive region is extended toward the aromatic H-atom *ortho* to the OH substituent, thus also adequate for interacting with electron rich species. This agrees well with the H-bonds described in **Figs. 5** and **6** for **5a,b**. The MEP values are also positive at the H-atoms of the alkyl chain, especially those closer to the tetrazole ring. The minimum MEP value is located, as expected, at the N-atoms of the tetrazole ring, ranging from -32 to -36 kcal/mol. Interestingly, the H-bonds observed in the solid state of compounds **5a,b** are established between the most positive and negative parts of the molecule. Finally, the MEP surface also reveals that the phenolic O-atom presents a moderately negative value of -21 kcal/mol. It is interesting to highlight that the MEP is negative over the phenolic ring (-12 kcal/mol) and negligible over the tetrazole ring. Therefore, it is expected that the antiparallel arrangement of these molecules to form π -stacking assemblies to minimize possible electrostatic repulsions between the phenolic rings.

Fig. 18 shows two selected dimers (H-bonded and π -stacking) retrieved from the X-ray structures of compounds **5a,b** and one dimer of compound **5c** along with their corresponding binding energies. Moreover, the QTAIM distributions of critical points (CPs)

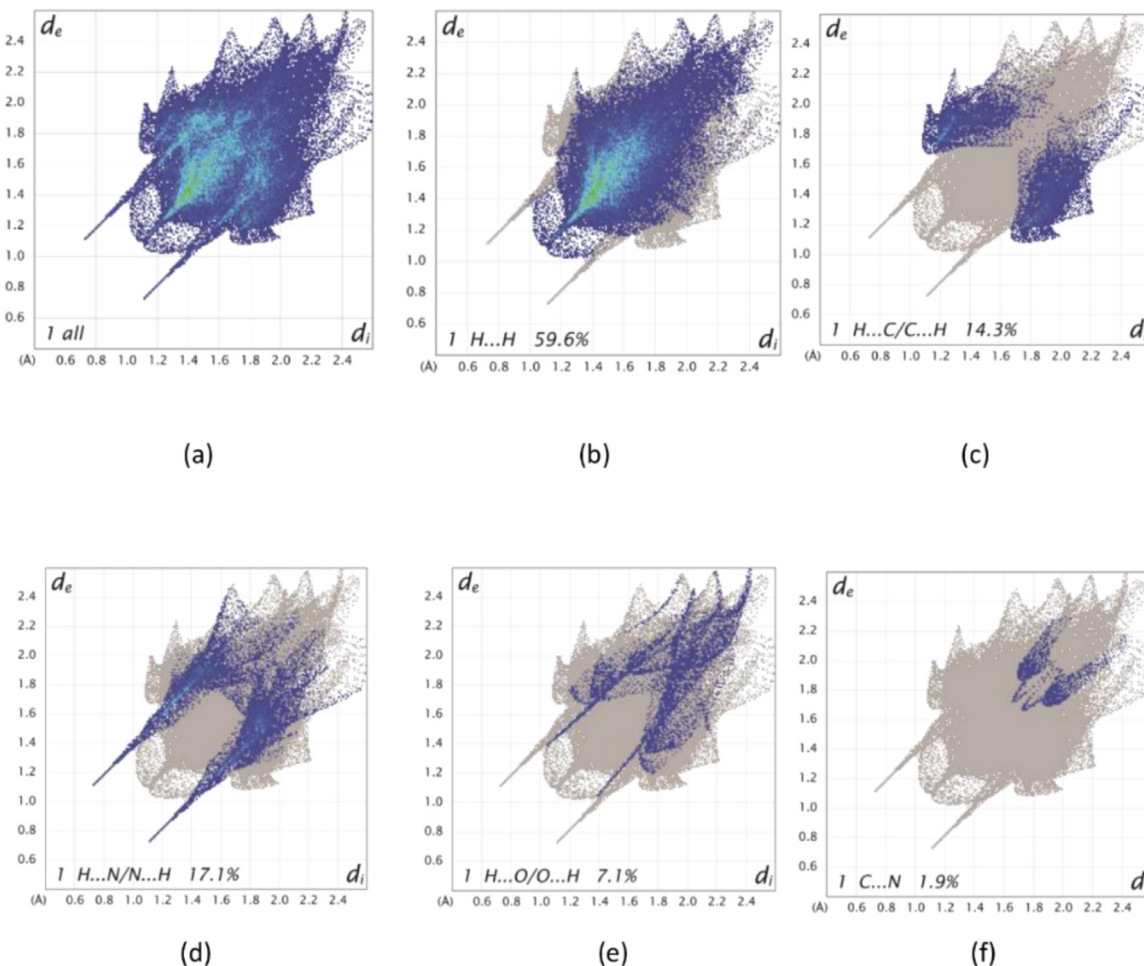


Fig. 12. Full two-dimensional fingerprint plots for the asymmetric unit of **5a**, (a), together with (b)-(f) separate contact types and included surface areas for the individual contacts. These are found to be H...H, H...C/C...H, H...N/N...H, H...O/O...H and C...N contacts.

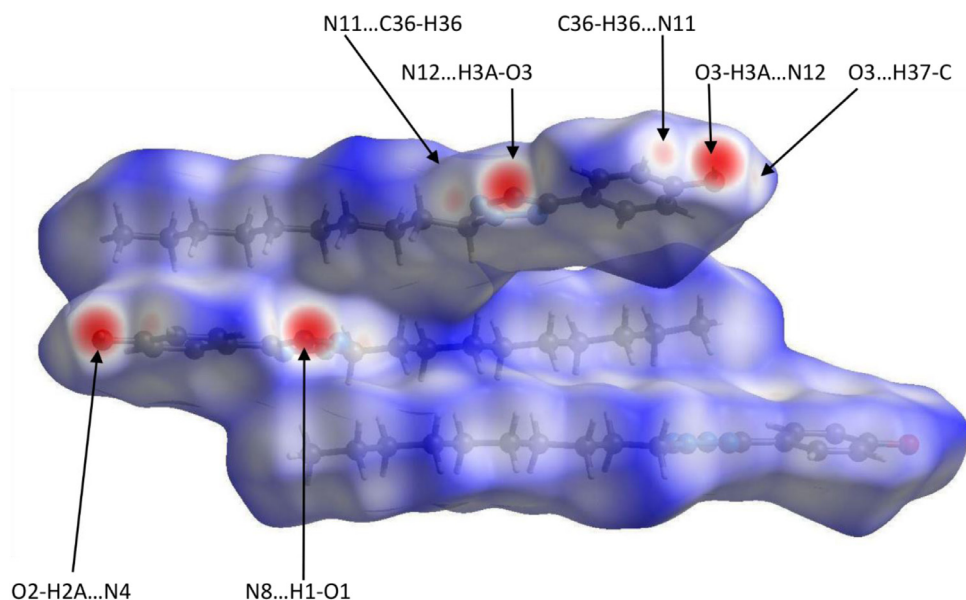


Fig. 13. Hirshfeld surfaces for the three molecules that comprise the asymmetric unit of **5b**, mapped over d_{norm} in the range -0.6289 to 1.7104 a.u.

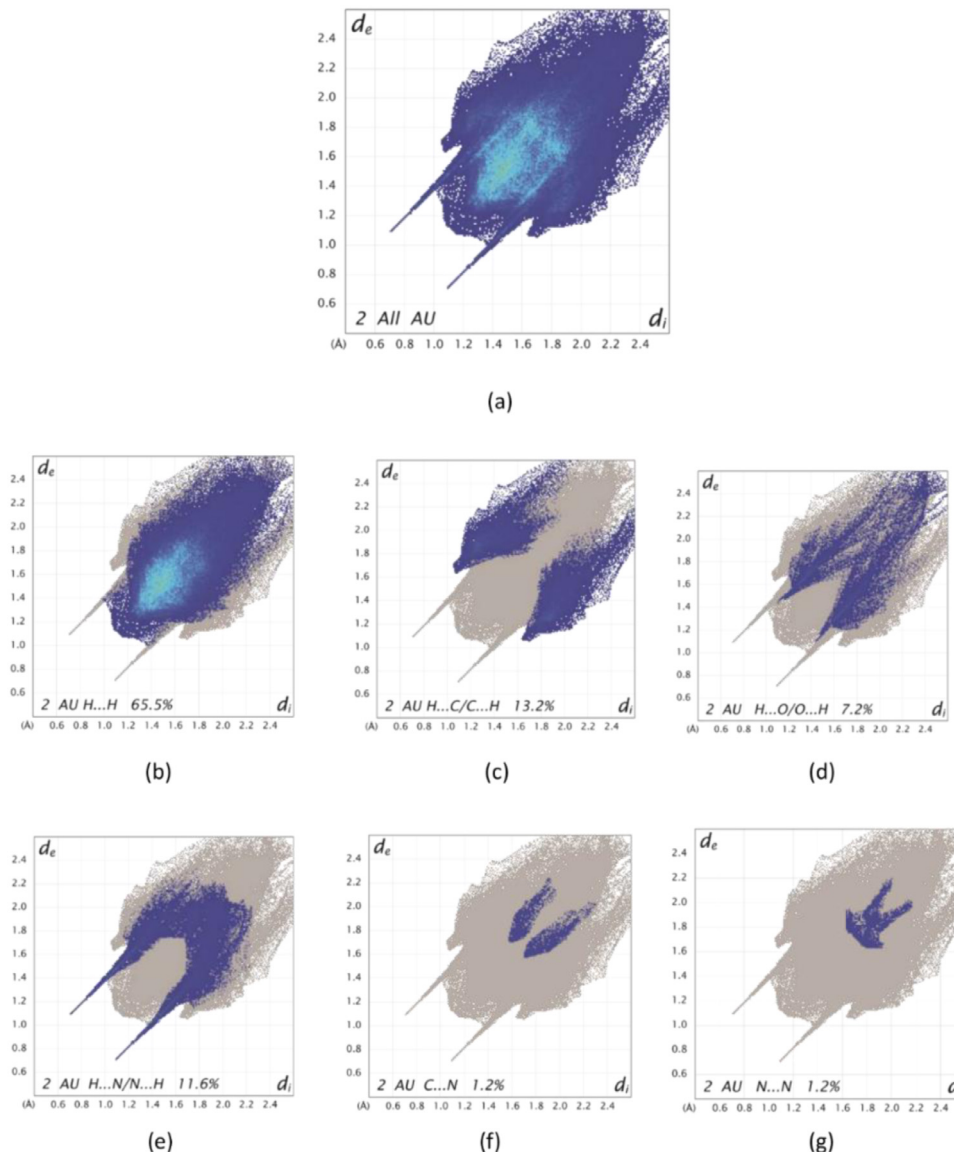


Fig. 14. Two-dimensional fingerprint plots for the asymmetric unit of **5b**, (a), together with (b)-(g) separate contact types and included surface areas for the individual contacts. Minor contacts contributing less than 1% to the total surface area are not shown here but, for completeness, are shown in Table 3. The secondary contacts shown here are H...H, H...C/C...H, H...N/N...H, H...O/O...H and C...N and N...N contacts.

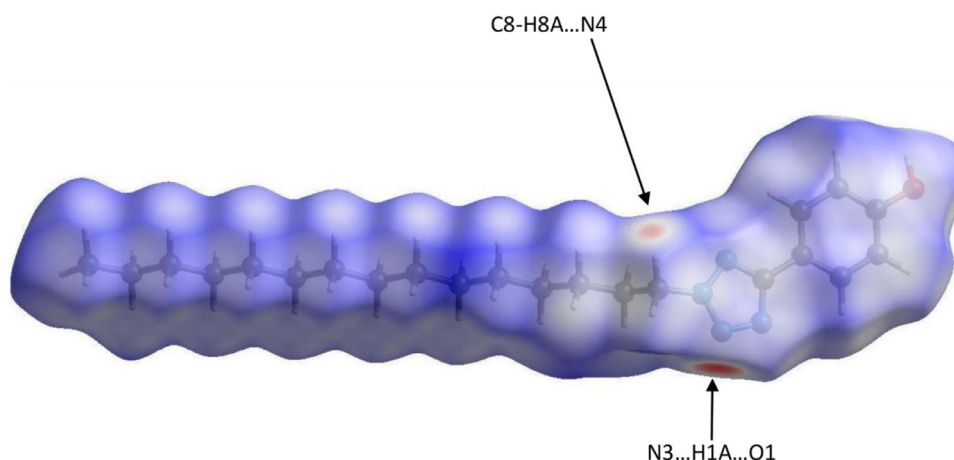


Fig. 15. Hirshfeld surface of the asymmetric unit of **5c**, mapped over d_{norm} in the range -0.5421 to 1.5181 a.u.

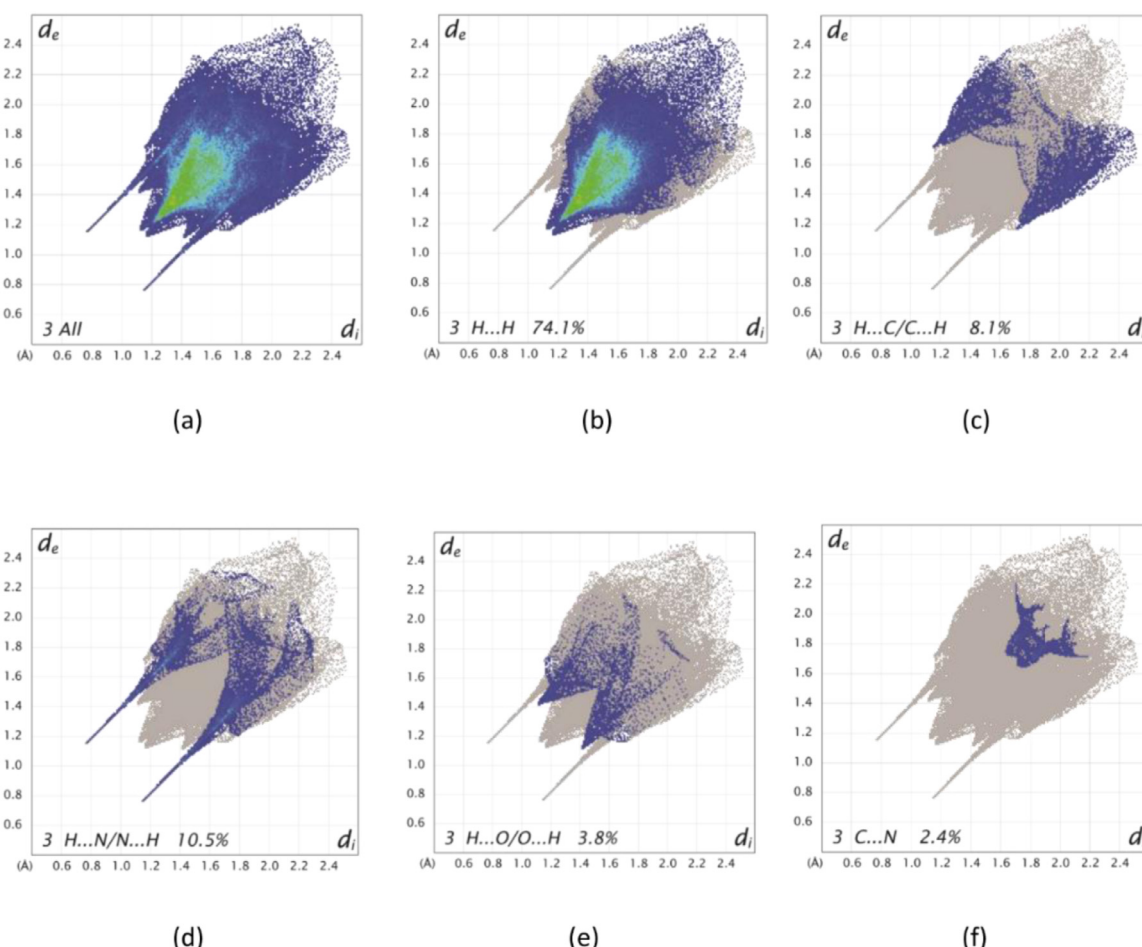


Fig. 16. Two-dimensional fingerprint plots for **5c**, (a), together with (b)-(f) separate contact types and included surface areas for the individual contacts. Minor contacts contributing less than 1% to the total surface area is not shown here but, for completeness, is shown in Table 3. The secondary contacts shown here are H...H, H...C/C...H, H...N/N...H and H...O/O...H and C...N contacts.

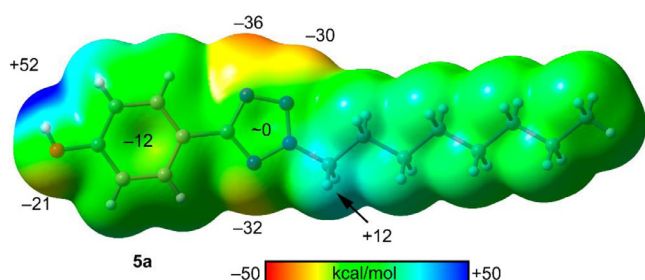


Fig. 17. MEP surface (0.001 a.u.) of **5a** at the PBE1PBE-D3/def2-TZVP level of theory. The values at selected points of the surfaces are given in kcal/mol.

and bond paths overlapped with the NCIplot surfaces of all complexes are also indicated. This type of analysis has been recently used to analyze a variety of interactions [97–99]. The H-bonded dimers of compounds **5a** and **5b** present similar energies ($\Delta E_1 = -9.4$ kcal/mol and $\Delta E_3 = -8.9$ kcal/mol, respectively) which are largely due to the formation of three concurrent H-bonds. Each H-bond is characterized by a bond CP (red sphere) and bond path interconnecting the H and N/O-atoms. The NCIplot also shows the corresponding isosurfaces, which are blue for the O-H...N4 H-bond and green for the C-H...O/N H-bonds, thus confirming their strong and weak nature, respectively. We have estimated the contribution of the strong H-bond by using the value of the kinetic energy density at the bond CP ($E = 0.5 \times V_r$). These values are also indicated in Fig. 18 and reveal that the O-H...N4 H-bond disso-

ciation energy is 5.4 kcal/mol in **5a** and 6.1 kcal/mol in **5b**, thus confirming their stronger nature. The π -stacking dimers of compounds **5a** and **5b** are shown in Figs. 18b and 18d, respectively. The dimerization energies are very similar ($\Delta E_2 = -12.0$ kcal/mol and $\Delta E_4 = -11.8$ kcal/mol, for **5a** and **5b** respectively); however, the NCIplot surface and QTAIM distribution of CPs reveal some interesting differences. In both compounds the π - π stacking is characterized by two bond CPs that interconnect two atoms of the tetrazole rings, however the NCIplot shows that the overlap of the π systems is significantly greater in **5b** (larger green isosurface between the tetrazole rings) than in **5a**. On the contrary, the C-H... π interactions are characterized by larger isosurfaces in compound **5a** than in **5b**. Therefore, π -stacking seems to dominate in **5b** and C-H... π interactions dominate in **5a**. Each C-H... π interaction is also confirmed by the QTAIM analysis that shows the existence of a bond CP that connects the H-atom to a C-atom of the aromatic ring. In general, both combinations of π -stacking and C-H... π interactions observed in **5a** and **5b** agree well with the MEP analysis, since the π -stacking involves the tetrazole ring (negligible MEP over the center of the ring) and the C-H... π interaction involves the electron rich phenol ring. Finally, the dimerization energy of H-bonded dimer of **5c** presents weaker interaction energy ($\Delta E_5 = -6.8$ kcal/mol), because only the O-H...N3 H-bond is established. Both the QTAIM and NCIplot index evidence the existence of an additional C-H...H-C interaction that is characterized by a small green isosurface and a bond CP connecting both H-atoms.

Finally, the different π -stacking assembly observed in compound **5c** (Fig. 19) has also been analyzed energetically. In the

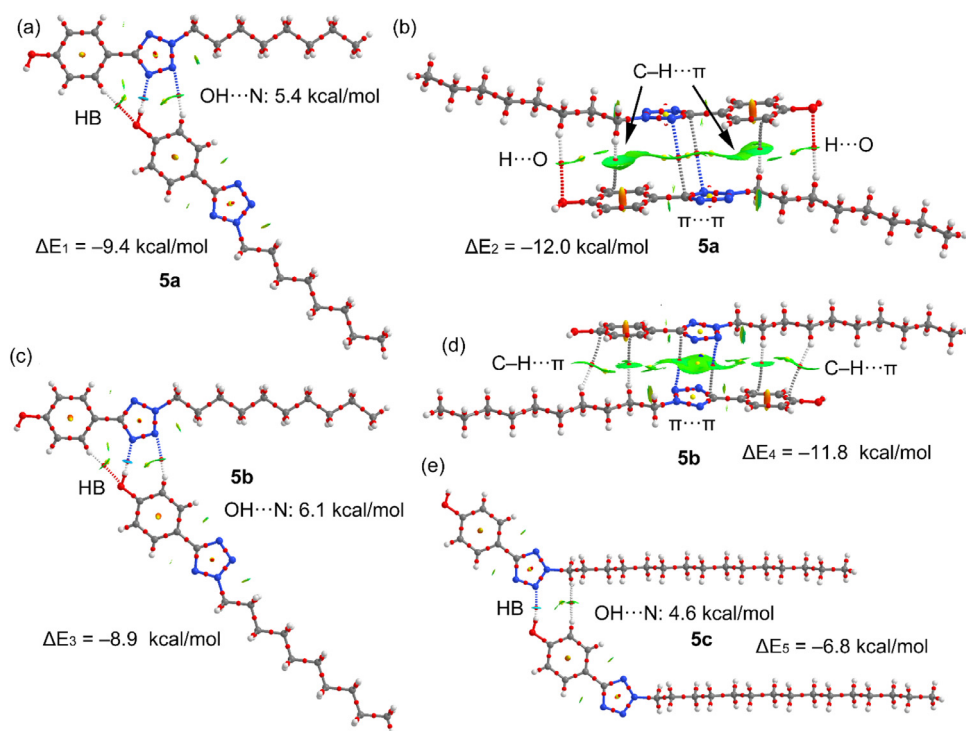


Fig. 18. QTAIM distribution of bond and ring CPs (red and yellow spheres, respectively) and the NCIplot isosurface using the gradient cut-off of 0.5 a.u. and color scale $-0.04 < \rho < 0.04$ a.u. for the dimers of **5a** (a,b), **5b** (c,d), **5c** (e). The interaction energies are also indicated.

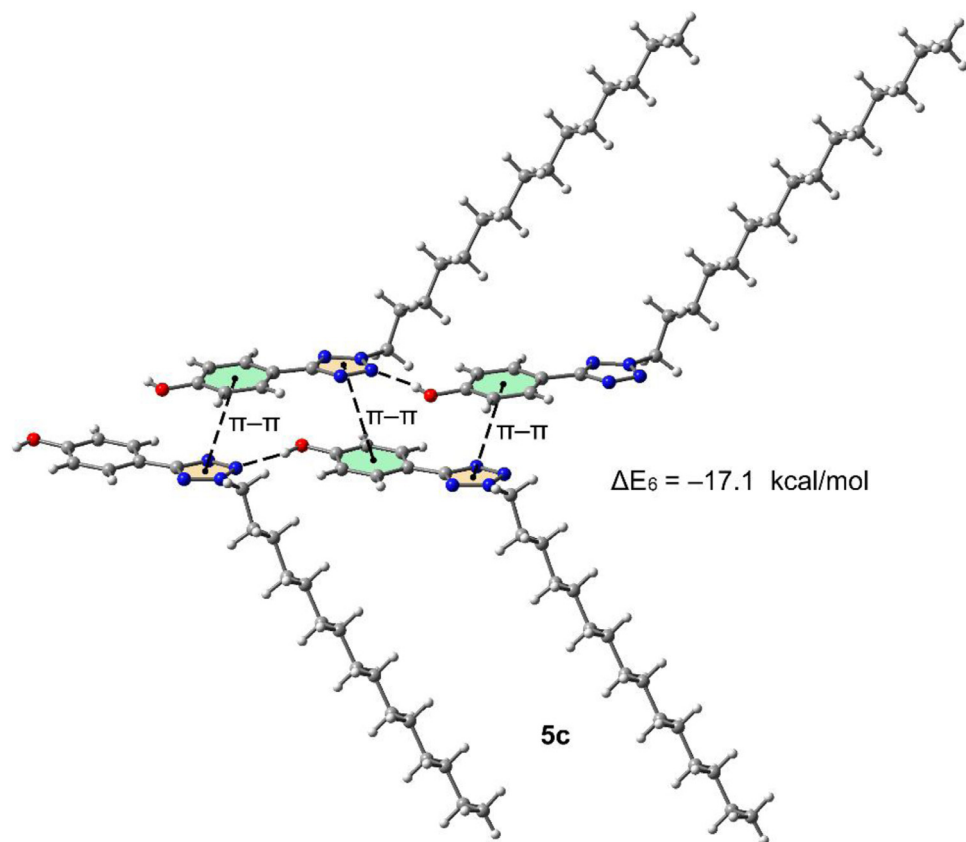


Fig. 19. Partial view of the X-ray of **5c** with indication of the $\pi-\pi$ interactions and the dimerization energy [2 x Dimer(HB) \rightarrow Tetramer].

tetramer shown in Fig. 19, the tetrazole and phenol rings stack and a total of three π - π interactions are established. The dimerization energy (the H-bonded dimer has been considered as a monomeric specie for the calculation of ΔE_6) is -17.1 kcal/mol that is significantly stronger than those π -stacking of compounds **5a** and **5b** (Fig. 18), thus compensating the weaker H-bond in **5c**.

4. Concluding remarks

In summary, the present study reports the efficient synthesis of substituted tetrazole structures that were characterized by spectro-analytical methods and X-ray diffraction analysis. The sufficient structural similarity within all the three molecules incorporating a tetrazole ring bearing beautifully ordered linear octyl **5a**, decyl **5b**, and pentadecyl **5c** chains at N-2 position and a phenol ring system at the 5-position allowed the formation of supramolecular assemblies through various non-covalent interactions. The conspicuous role of hydrogen bonding (C-H... π , O-H...N, C-H...N, C-H...O) and π ... π stacking was realized in the stabilization of the solid-state conformations. Further details of the intermolecular interactions in the three molecules were obtained using Hirshfeld surface analysis and their energetic features by DFT calculations. Moreover, the combined QTAIM/NClplot analyses further characterize the interactions and provide valuable information regarding the relative importance of each non-covalent contact.

Declaration of Competing Interest

The authors declare that they have no known competing financial interests or personal relationships that could have appeared to influence the work reported in this paper.

Acknowledgements

H.A. is grateful to the Higher Education Commission of Pakistan for financial support under the Indigenous 5000 PhD Fellowship program and SRGP Grant No. 2470. J.S. thanks the Chemistry Department, University of Otago for support of his work. We thank the MICIU/AEI from Spain for financial support (project number CTQ2017-85821-R, FEDER funds). We are also grateful to the CTI (UIB) for free allocation of computer time.

Supplementary material

Supplementary material associated with this article can be found, in the online version, at doi:10.1016/j.molstruc.2020.129425.

References

- [1] U. Bhatt, Five-Membered Heterocycles with Four Heteroatoms: tetrazoles, in: Modern Heterocyclic Chemistry, Wiley-VCH Verlag GmbH & Co. KGaA, 2011, pp. 1401–1430.
- [2] G.I. Koldobskii, R.B. Kharbash, Russ. J. Org. Chem. 39 (2003) 453–470.
- [3] G.I. Koldobskii, Russ. J. Org. Chem. 42 (2006) 469–486.
- [4] J. Roh, K. Vavrova, A. Hrabalek, Eur. J. Org. Chem. (2012) 6101–6118.
- [5] , in: First Symposium on Chemical-Biological Correlation, May 26–27, 1050, National Academy of Sciences, National Research Council, 1950, p. 1951.
- [6] G.F. Holland, J.N. Pereira, J. Med. Chem. 10 (1967) 149–154.
- [7] S.K. Figdor, M.S. von Wittewien, J. Med. Chem. 10 (1967) 1158–1159.
- [8] K. Kubo, Y. Kohara, Y. Yoshimura, Y. Inada, Y. Shibota, Y. Furukawa, T. Kato, K. Nishikawa, T. Naka, J. Med. Chem. 36 (1993) 2343–2349.
- [9] J.L. Kraus, Pharmacol. Res. Commun. 15 (1983) 183–189.
- [10] M.L. Quan, C.D. Ellis, M.Y. He, A.Y. Liauw, F.J. Woerner, R.S. Alexander, R.M. Knabb, P.Y.S. Lam, J.M. Luetgen, P.C. Wong, M.R. Wright, R.R. Wexler, Bioorg. Med. Chem. Lett. 13 (2003) 369–373.
- [11] E. Muraglia, O.D. Kinzel, R. Laufer, M.D. Miller, G. Moyer, V. Munshi, F. Orvieto, M.C. Palumbi, G. Pescatore, M. Rowley, P.D. Williams, V. Summa, Bioorg. Med. Chem. Lett. 16 (2006) 2748–2752.
- [12] R.S. Upadhyaya, S. Jain, N. Sinha, N. Kishore, R. Chandra, S.K. Arora, Eur. J. Med. Chem. 39 (2004) 579–592.
- [13] T.R. Burke, Z.J. Yao, Y. Gao, J.X. Wu, X. Zhu, J.H. Luo, R. Guo, D. Yang, Bioorg. Med. Chem. 9 (2001) 1439–1445.
- [14] S. Kumar, A.L. Pearson, R.F. Pratt, Bioorg. Med. Chem. 9 (2001) 2035–2044.
- [15] S.A.F. Rostom, H.M.A. Ashour, H.A.A. El. Razik, H. Abd El Fattah, N.N. El-Din, Bioorg. Med. Chem. 17 (2009) 2410–2422.
- [16] V.V. Zarubaev, E.L. Golod, P.M. Anfimov, A.A. Shtro, V.V. Sarayev, A.S. Gavrilov, A.V. Logvinov, O.I. Kiselev, Bioorg. Med. Chem. 18 (2010) 839–848.
- [17] J. Li, S.Y. Chen, J.J. Li, H. Wang, A.S. Hernandez, S. Tao, C.M. Musial, F. Qu, S. Swartz, S.T. Chao, N. Flynn, B.J. Murphy, D.A. Slusarchyk, R. Seethala, M. Yan, P. Slep, G. Grover, M.A. Smith, B. Beehler, L. Giupponi, K.E. Dickinson, H. Zhang, W.G. Humphreys, B.P. Patel, M. Schwinden, T. Stouch, P.T.W. Cheng, S.A. Biller, W.R. Ewing, D. Gordon, J.A. Robl, J.A. Tino, J. Med. Chem. 50 (2007) 5890–5893.
- [18] T. Kambe, B.E. Correia, M.J. Niphakis, B.F. Cravatt, J. Am. Chem. Soc. 136 (2014) 10777–10782.
- [19] S. Wu, A. Fluxe, J. Sheffer, J.M. Janusz, B.E. Blass, R. White, C. Jackson, R. Hedges, M. Murawsky, B. Fang, G.M. Fadayel, M. Hare, L. Djandjighian, Bioorg. Med. Chem. Lett. 16 (2006) 6213–6218.
- [20] J. Li, S.Y. Chen, S. Tao, H. Wang, J.J. Li, S. Swartz, C. Musial, A.A. Hernandez, N. Flynn, B.J. Murphy, B. Beehler, K.E. Dickinson, L. Giupponi, G. Grover, R. Seethala, P. Slep, D. Slusarchyk, M. Yan, W.G. Humphreys, H. Zhang, W.R. Ewing, J.A. Robl, D. Gordon, J.A. Tino, Bioorg. Med. Chem. Lett. 18 (2008) 1825–1829.
- [21] S.Y. Kang, S.H. Lee, H.J. Seo, M.E. Jung, K. Ahn, J. Kim, J. Lee, Bioorg. Med. Chem. Lett. 18 (2008) 2385–2389.
- [22] J.J. Li, H. Wang, J. Li, F. Qu, S.G. Swartz, A.S. Hernández, S.A. Biller, J.A. Robl, J.A. Tino, D. Slusarchyk, R. Seethala, P. Slep, M. Yan, G. Grover, N. Flynn, B.J. Murphy, D. Gordon, Bioorg. Med. Chem. Lett. 18 (2008) 2536–2539.
- [23] G. Ortar, A. Schiano Morello, M.G. Cascio, L. De Petrocellis, A. Ligresti, E. Morera, M. Nalli, V. Di Marzo, Bioorg. Med. Chem. Lett. 18 (2008) 2820–2824.
- [24] P.D. Boatman, T.O. Schrader, M. Kasem, B.R. Johnson, P.J. Skinner, J.-K. Jung, J. Xu, M.C. Cherrier, P.J. Webb, G. Semple, C.R. Sage, J. Knudsen, R. Chen, A.K. Taggart, E. Carballo-Jane, J.G. Richman, Bioorg. Med. Chem. Lett. 20 (2010) 2797–2800.
- [25] V.V. Filichev, M.V. Jasko, A.A. Malin, V.Y. Zubarev, V.A. Ostrovskii, Tetrahedron Lett. 43 (2002) 1901–1903.
- [26] G. Garipova, A. Gautier, S.R. Piettre, Tetrahedron 61 (2005) 4755–4759.
- [27] G. Roman, M.N. Rahman, D. Vukomanovic, Z.C. Jia, K. Nakatsu, W.A. Szarek, Chem. Biol. Drug Des. 75 (2010) 68–90.
- [28] D.S. Wishart, DrugBank: A Comprehensive Resource for in Silico Drug Discovery and Exploration, Nucleic Acids Res 34 (2006) D668–D672.
- [29] C.G. Neochoritis, T. Zhao, A. Dömling, Chem. Rev. 119 (2019) 1970–2042.
- [30] C. Liljebris, S.D. Larsen, D. Ogg, B.J. Palazuk, J.E. Bleasdale, J. Med. Chem. 45 (2002) 1785–1798.
- [31] E. Meyer, C. Zucco, H. Gallardo, J. Mater. Chem. 8 (1998) 1351–1354.
- [32] H. Gallardo, I.M. Begnini, A. Neves, I. Vencato, J. Braz. Chem. Soc. 11 (2000) 274–280.
- [33] D.R. dos Santos, A.G.S. de Oliveira, R.L. Coelho, I.M. Begnini, R.F. Magnago, L. da Silva, ARKIVOC xvii (2008) 157–166.
- [34] H. Wang, W. Wang, W.J. Jin, Chem. Rev. 116 (2016) 5072–5104.
- [35] L. Brammer, Faraday Discuss 203 (2017) 485–507.
- [36] L.C. Gilday, S.W. Robinson, T.A. Barendt, M.J. Langton, B.R. Mullaney, P.D. Beer, Chem. Rev. 115 (2015) 7118–7195.
- [37] A. Bauzá, T.J. Mooibroek, A. Frontera, ChemPhysChem 16 (2015) 2496–2517.
- [38] L.M. Salonen, M. Ellermann, F. Diederich, Angew. Chem. Int. Ed. 50 (2011) 4808–4842.
- [39] D. Paolonti, J. Rubio-Magnieto, S. Cantel, J. Martinez, P. Dumy, M. Surin, S. Ulrich, Chem. Commun. 50 (2014) 14257–14260.
- [40] C. Estarellas, A. Frontera, D. Quiñónero, P.M. Deyà, Angew. Chem. Int. Ed. 50 (2011) 415–418.
- [41] M.J. Katz, K. Sakai, D.B. Leznoff, Chem. Soc. Rev. 37 (2008) 1884–1895.
- [42] S. Yamada, N. Sako, M. Okuda, A. Hozumi, CrystEngComm 15 (2013) 199–205.
- [43] A. Sasmal, A. Bauzá, A. Frontera, C. Rizzoli, C. Desplanches, L.J. Charbonnière, S. Mitra, Dalton Trans 43 (2014) 6195–6211.
- [44] I. Caracelli, I. Haiduc, J. Zukerman-Schpector, E.R.T. Tieckink, Coord. Chem. Rev. 257 (2013) 2863–2879.
- [45] F. Orvay, A. Bauzá, M. Barceló-Olivier, A. García-Raso, J.J. Fiol, A. Costa, E. Molins, I. Mata, A. Frontera, CrystEngComm 16 (2014) 9043–9053.
- [46] G.R. Desiraju, Chem. Commun. (1997) 1475–1482.
- [47] G.R. Desiraju, J. Chem. Sci. 122 (2010) 667–675.
- [48] P.A. Gale, Chem. Commun. 47 (2011) 82–86.
- [49] M. Wenzel, J.R. Hiscock, P.A. Gale, Chem. Soc. Rev. 41 (2012) 480–520.
- [50] P.A. Gale, R. Quesada, Coord. Chem. Rev. 250 (2006) 3219–3244.
- [51] H.J. Schneider, Angew. Chem. Int. Ed. 48 (2009) 3924–3977.
- [52] H.J. Schneider, A. Yatsimirski, Principles and Methods in Supramolecular Chemistry, Wiley, Chichester, 2000.
- [53] G.R. Desiraju, T. Steiner, The Weak Hydrogen Bond in Structural Chemistry and Biology, OUP, Oxford, 1999.
- [54] P. Metrangolo, H. Neukirch, T. Pilati, G. Resnati, Acc. Chem. Res. 38 (2005) 386–395.
- [55] T.T. Bui, S. Dahaoui, C. Lecomte, G.R. Desiraju, E. Espinosa, Angew. Chem. Int. Ed. 48 (2009) 3838–3841.
- [56] A. Hazari, L.K. Das, A. Bauza, A. Frontera, A. Ghosh, Dalton Trans 43 (2014) 8007–8015.
- [57] P. Seth, A. Bauza, A. Frontera, A. Ghosh, Inorg. Chem. Commun. 41 (2014) 1–5.
- [58] A. Bhattacharyya, P.K. Bhaumik, A. Bauza, P.P. Jana, A. Frontera, M.G.B. Drew, S. Chattopadhyay, RSC Adv 4 (2014) 58643–58651.
- [59] H.S. Jena, RSC Adv 4 (2014) 3028–3044.

- [60] H.S. Jena, Inorg. Chim. Acta 410 (2014) 156–170.
- [61] S. Naiya, M.G.B. Drew, C. Estarellas, A. Frontera, A. Ghosh, Inorg. Chim. Acta 363 (2010) 3904–3913.
- [62] C. Murcia-García, A. Bauzá, G. Schnakenburg, A. Frontera, R. Streubel, CrystEngComm 17 (2015) 1769–1772.
- [63] I. Khan, A. Ibrar, J. Simpson, CrystEngComm 16 (2014) 164–174.
- [64] I. Khan, P. Panini, S.U.-D. Khan, U.A. Rana, H. Andleeb, D. Chopra, S. Hameed, J. Simpson, Cryst. Growth Des. 16 (2016) 1371–1386.
- [65] R. Shukla, I. Khan, A. Ibrar, J. Simpson, D. Chopra, CrystEngComm 19 (2017) 3485–3498.
- [66] H. Andleeb, I. Khan, A. Franconetti, M.N. Tahir, J. Simpson, S. Hameed, A. Frontera, CrystEngComm 21 (2019) 1780–1793.
- [67] M. Tariq, S. Hameed, I.H. Bechtold, A.J. Bortoluzzi, A.A. Merlo, J. Mater. Chem., C 1 (2013) 5583–5593.
- [68] BrukerAPEX2 and SAINT, Bruker AXS Inc., Madison, Wisconsin, USA, 2007.
- [69] BrukerSADABS, Bruker AXS Inc., Madison, Wisconsin, USA, 2005.
- [70] G.M. Sheldrick, Acta Cryst A64 (2008) 112–122.
- [71] G.M. Sheldrick, Acta Cryst C71 (2015) 3–8.
- [72] K.A. Hunter, J. Simpson, TITAN2000, University of Otago, New Zealand, 1999.
- [73] C.F. Macrae, I.J. Bruno, J.A. Chisholm, P.R. Edgington, P. McCabe, E. Pidcock, L. Rodriguez-Monge, R. Taylor, J. van de Streek, P.A. Wood, J. Appl. Cryst. 41 (2008) 466–470.
- [74] A.L. Spek, Acta Cryst D65 (2009) 148–155.
- [75] L.J. Farrugia, J. Appl. Cryst. 45 (2012) 849–854.
- [76] M.J. Frisch, G.W. Trucks, H.B. Schlegel, G.E. Scuseria, M.A. Robb, J.R. Cheeseman, G. Scalmani, V. Barone, G.A. Petersson, H. Nakatsuji, X. Li, M. Caricato, A.V. Marenich, J. Bloino, B.G. Janesko, R. Gomperts, B. Mennucci, H.P. Hratchian, J.V. Ortiz, A.F. Izmaylov, J.L. Sonnenberg, D. Williams-Young, F. Ding, F. Lipparini, F. Egidi, J. Goings, B. Peng, A. Petrone, T. Henderson, D. Ranasinghe, V.G. Zakrzewski, J. Gao, N. Rega, G. Zheng, W. Liang, M. Hada, M. Ehara, K. Toyota, R. Fukuda, J. Hasegawa, M. Ishida, T. Nakajima, Y. Honda, O. Kitao, H. Nakai, T. Vreven, K. Throssell, J.A. Montgomery Jr., J.E. Peralta, F. Ogliaro, M.J. Bearpark, J.J. Heyd, E.N. Brothers, K.N. Kudin, V.N. Staroverov, T.A. Keith, R. Kobayashi, J. Normand, K. Raghavachari, A.P. Rendell, J.C. Burant, S.S. Iyengar, J. Tomasi, M. Cossi, J.M. Millam, M. Klene, C. Adamo, R. Cammi, J.W. Ochterski, R.L. Martin, K. Morokuma, O. Farkas, J.B. Foresman, D.J. Fox, Gaussian 16, Revision A.01, Gaussian, Inc., Wallingford CT, 2016.
- [77] S.F. Boys, F. Bernardi, Mol. Phys. 19 (1970) 553–566.
- [78] D. Rappoport, F. Furche, J. Chem. Phys. 133 (2010) 134105.
- [79] F. Weigend, R. Ahlrichs, Phys. Chem. Chem. Phys. 7 (2005) 3297–3305.
- [80] J.P. Perdew, K. Burke, M. Ernzerhof, Phys. Rev. Lett. 77 (1996) 3865–3868.
- [81] J.P. Perdew, M. Ernzerhof, K. Burke, J. Chem. Phys. 105 (1996) 9982–9985.
- [82] S. Grimme, J. Comput. Chem. 27 (2006) 1787–1799.
- [83] S. Grimme, J. Antony, S. Ehrlich, H. Krieg, J. Chem. Phys. 132 (2010) 154104.
- [84] E.R. Johnson, S. Keinan, P. Mori-Sánchez, J. Contreras-García, A.J. Cohen, W. Yang, J. Am. Chem. Soc. 132 (2010) 6498–6506.
- [85] J. Contreras-García, E.R. Johnson, S. Keinan, R. Chaudret, J.-P. Piquemal, D.N. Beratan, W. Yang, J. Chem. Theory Comput. 7 (2011) 625–632.
- [86] Todd A. Keith, AIMAll (Version 19.10.12), TK Gristmill Software, Overland Park KS, USA, 2019 (aim.tkgristmill.com).
- [87] C.R. Groom, L.J. Bruno, M.P. Lightfoot, S.C. Ward, Acta Cryst B72 (2016) 171–179.
- [88] Q. Zhang, J.-Y. Li, Y.-H. Yu, G.F. Hou, Jin-Sheng Gao, J. S., Chin. J. Struct. Chem. 34 (2016) 818–826.
- [89] A. Mohan, P. Ramesh, D. Saravanan, M.N. Ponnuswamy, Acta Cryst E66 (2010) 0998.
- [90] J.G. Malecki, J. G. (2017). CSD Private Communication.
- [91] B.W. Skelton, M.J. Piggott and A. Toynton, (2018). CSD Private Communication.
- [92] A. Fleming, F. Kelleher, M.F. Mahon, J. McGinley, V. Prajapati, Tetrahedron 61 (2005) 7002–7011.
- [93] A.D. Bond, A. Fleming, J. Gaire, F. Kelleher, J. McGinley, V. McKee, Tetrahedron 65 (2009) 7942–7947.
- [94] A.D. Bond, A. Fleming, F. Kelleher, J. McGinley, V. Prajapati, Tetrahedron 62 (2006) 9577–9581.
- [95] M.A. Spackman, D. Jayatilaka, CrystEngComm 11 (2009) 19–32.
- [96] M.J. Turner, J.J. McKinnon, S.K. Wolff, D.J. Grimwood, P.R. Spackman, D. Jayatilaka, M.A. Spackman, CrystalExplorer17, University of Western Australia, Netherlands, Western Australia, 2017 <http://hirshfeldsurface.net>.
- [97] L. Bofill, D. de Sande, R. Barbas, A. Frontera, R. Prohens, CrystEngComm 22 (2020) 4680–4684.
- [98] A. Bauzá, I. Alkorta, J. Elguero, T.J. Mooibroek, A. Frontera, Angew. Chem. Int. Ed. 59 (2020) 17482–17487.
- [99] N.S. Soldatova, P.S. Postnikov, V.V. Suslonov, T. Yu. Kissler, D.M. Ivanov, M.S. Yusubov, B. Galmes, A. Frontera, V. Yu. Kukushkin, Org. Chem. Front. 7 (2020) 2230–2242.